AD-A194 118 MODELING OF ATOMIC PROCESSES IN X-RAY LASER PLASMAS(U) 1/1
BERKELEY RESEARCH ASSOCIATES INC CA MAR 88
BRA-88-W030R N00014-86-C-2454

UNCLASSIFIED F/G 20/5 NL

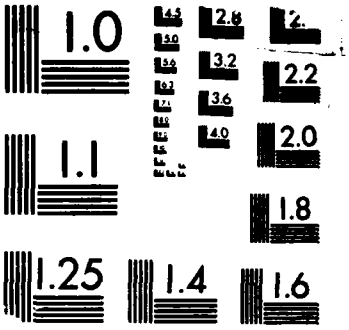

BERKELEY RESEARCH
ASSOCIATES, INC.

BRA-88-W030R
March 1988

MODELING OF ATOMIC PROCESSES IN X-RAY LASER PLASMAS

Final Report

Contract N00014-86-C-2454

for

Naval Research Laboratory
Washington, DC 20375

by

Berkeley Research Associates, Inc.
P. O. Box 241
Berkeley, CA 94701

BRA-88-W030R
March 1988

MODELING

OF

ATOMIC PROCESSES

IN

X-RAY LASER PLASMAS

Final Report

Contract N00014-86-C-2454

for

Naval Research Laboratory
Washington, DC 20375

by

Berkeley Research Associates, Inc.
P.O. Box 241
Berkeley, California 94701

I. INTRODUCTION

This final report covers research carried out in conjunction with the Naval Research Laboratory for the performance period 19 September 1986 to 19 September 1987 for Contract N00014-86-C-2454. The research involved was primarily to investigate the interaction of atomic systems with an applied laser beam and to compute photoabsorption cross-sections of ions of specific configurations such as argon and xenon. These cross-sections were calculated at various incident photon energies, and the respective time-dependent atomic polarizabilities were examined. Comparisons between calculated and experimentally determined cross-sections were made, and laser-atom interactions were examined as well.

For modeling of radiative properties of x-ray laser plasmas, a variety of atomic data are needed as input. In the context of photopumping schemes for x-ray lasers, photoionization and photoexcitation of multielectron atoms and ions (and the inverse process of radiative recombination) are particularly important. The electronic population inversion of atomic states necessary for lasing are brought about by the interplay of these atomic processes.

Accurate calculation of photoionization and photoexcitation cross-sections and rates are useful in a variety of investigations in plasma physics, astrophysics and atomic physics. In the modeling of radiation spectra of hot plasmas (via the detailed configuration rate equation for example), these data are required along with the other bound-bound, bound-free and free-free processes. As another example, computation of opacities of plasmas for diagnostic and target response effects require these data as input. In view of these different applications, there is a need for realistic modeling of these processes to generate accurate data for a variety of atoms and ions.

Most of the existing calculations of photoionization cross-sections were done using the single electron or the independent particle model (IPA). In this model, the energy levels and wave functions of the atom or ion are first calculated using the Hartree-Fock (HF) method. The interaction of the incident electromagnetic radiation with the atom (or ion) is treated via the first order perturbation theory[1].

Comparison of experimental data with the IPA calculations shows that for some simple systems such as a neutral, few-electron atom (lithium for example), there is a qualitative and sometimes quantitative agreement. However, for many electron atoms (xenon for example), substantial discrepencies are found between experimental and IPA data[1].

In our work, we used the time-dependent linear response approximation within the framework of the relativistic density functional method (DFM)[2,3,4] to treat the problem of photoionization. This method incorporates several advantages over the HF-method. For example, the HF-method is non-local and computationally very elaborate. The DFM, on the other hand, deals only with a set of local equations and is therefore far less complex computationally. Despite its local nature, however, extensive applications of the DFM have proven it to be fairly accurate in obtaining energy levels, wave functions, etc.

In cases in which there are high Z atoms and relativistic treatments are required, the computational simplicity of the relativistic DFM versus the relativistic HF-methods is even more apparent. In the DFM, correlation effects of the bound electrons are accounted for in a simple way via the correlation potential[5]. The HF-method, on the other hand, does not take into account electron correlation, although it accounts for non-local exchange effects appropriately.

The independent particle model does not take into account the polarization effect of the atom brought about by the incident time-varying radiation field. In the linear response method within the DFM, this is treated adequately as will be seen from comparison with experimental data. In most experimental situations, the incident radiation from synchrotron sources or lasers have field strengths small compared to atomic field strengths. For those experimental conditions, the present model based on linear response is adequate and useful. For very strong applied fields, it is necessary to go beyond the linear response approximation and utilize a full time-dependent density functional approach. In the later part of the report, we will discuss this aspect briefly.

II. TECHNICAL DISCUSSION

A. THE METHOD OF CALCULATION

1. Isolated Atoms or Multielectron Ions

The first part of the calculation is to generate the energy-level spectrum and the wave functions of the particular atom or ion of specific configuration. This is done by using the local density functional method. In order to treat many-electron atoms (with high Z) appropriately, relativistic DFM equations are used. In this method, the following set of equations are solved self-consistently:

$$[c\alpha \cdot \mathbf{p} + c^2\beta + u(\mathbf{r})]\psi_i(\mathbf{r}) = E_i\psi_i(\mathbf{r}) \tag{1}$$

$$u(r) = -\frac{Z}{r} + \int \frac{\rho(\mathbf{r}')d\mathbf{r}'}{|\mathbf{r} - \mathbf{r}'|} + \frac{\partial}{\partial\rho(\mathbf{r})}[\rho(\mathbf{r})\epsilon_{xc}(\rho(\mathbf{r}))] \tag{2}$$

and

$$\rho(\mathbf{r}) = \sum_i f_i|\psi_i(\mathbf{r})|^2 \tag{3}$$

In the above, $\rho(\mathbf{r})$ is the electronic charge density of the atom, $\alpha's$ are the Dirac matrices and $f_i's$ are the integral occupation factors corresponding to the number of electrons in each state $\psi_i(r)$ with corresponding energy eigenvalue E_i. The atomic potential $u(r)$ contains, in addition to the nuclear and the electrostatic Hartree term, a contribution arising from the electron exchange and correlation effects. Also, ϵ_{xc} is the exchange-correlation energy of the electrons with the Gunnarsson-Lundquist (G-L) form[4] for exchange-correlation energy and potential is used in actual calculations. It is well known that reliable atomic data is obtained from the use of G-L exchange-correlation. Let us note that the use of integer occupation factors $f_i's$ for the given configuration distinguishes this model from the "average atom model" in which the occupation factors are taken to be those given by the statistical Fermi distribution function.

The orbital functions are four-component spinors. They are split into major and minor components

$$\psi(\mathbf{r}) = \begin{pmatrix} \psi^1(\mathbf{r}) \\ \psi^2(\mathbf{r}) \end{pmatrix} = \begin{pmatrix} (A(r)/r) i^l \Omega_{jlm}(\hat{r}) \\ (B(r)/r) i^l \Omega_{jl'm}(\hat{r}) \end{pmatrix} \tag{4}$$

where A and B are major and minor components of the radial functions, and Ω_{jlm} and $\Omega_{jl'm}$ are two-component Pauli spinors with the indicated numbers. The various quantum numbers are related by

$$l' = l + S, \quad j' = l + \frac{1}{2}, \quad S = l' - \frac{1}{2}S, \quad K = -S(j + \frac{1}{2}); \quad S = \pm 1 \tag{5}$$

The differential equations for A and B (in matrix form) are

$$\frac{d}{dr}\begin{pmatrix} A \\ B \end{pmatrix} = \begin{pmatrix} -\frac{K}{r} & \frac{(u-E-c^2)}{cs} \\ -\frac{(u-E-c^2)}{cs} & \frac{K}{r} \end{pmatrix}\begin{pmatrix} A \\ B \end{pmatrix} \tag{6}$$

Equations (1) - (6) are solved numerically to self-consistency to obtain the wave functions $\psi_i's$, the binding energies of each orbital E_i, the atomic charge density $\rho(\mathbf{r})$ and the self-consistent potential $u(\mathbf{r})$.

Now consider the effect of an incident time-varying radiation field $E(t) = E_o e^{i\omega t}$ on the atom. It induces a time-dependent atomic density deviation, $\delta p(\mathbf{r}, t)$, causing a time-dependent polarization effect. For the linear response method used here, it is convenient to work with the Fourier transform

$$\delta\rho(\mathbf{r}, t) = \frac{1}{2\pi}\int_{-\infty}^{\infty} \delta\rho(\mathbf{r}, \omega) e^{-i\omega t} d\omega \tag{7}$$

The net induced density due to the external plus the induced potential is

$$\delta\rho_{ind}(\mathbf{r}, \omega) = \int \chi(\mathbf{r}, \mathbf{r}', \omega)[V_{ext}(\mathbf{r}, \omega) + V_{ind}(\mathbf{r}, \omega)]d\mathbf{r}', \tag{8}$$

where the induced potential is given by

$$V_{ind}(\mathbf{r}, \omega) = \int \frac{\delta\rho(\mathbf{r}', \omega)}{\mathbf{r} - \mathbf{r}'} d\mathbf{r}' + \frac{\partial V_{xc}(\rho(\mathbf{r}))}{\partial\rho(\mathbf{r})}\delta\rho(\mathbf{r}, \omega) \tag{9}$$

The response function is given by

$$\chi(\mathbf{r},\mathbf{r}',\omega) = \sum_i f_i \psi_i^*(\mathbf{r})\psi_i(\mathbf{r}')G(\mathbf{r},\mathbf{r}',E_i+\omega) + \sum_i f_i \psi_i(\mathbf{r})\psi_i^*(\mathbf{r}')G^*(\mathbf{r},\mathbf{r}',E_i-\omega) \quad (10)$$

and thus involves the wave functions and energy levels of the atom. The Green's functions are solutions of the inhomogeneous Dirac equation

$$(c\alpha\cdot\rho + c^2\beta + u(r) - E)G(\mathbf{r},\mathbf{r}',E) = -\delta(\mathbf{r}-\mathbf{r}') \quad (11)$$

In actual calculation, angular decomposition of the Green's function in terms of spherical harmonics is done and the radial part is treated separately.

The frequency dependent polarizability $\alpha(\omega)$ is the ratio of the induced dipole moment to the external field:

$$\alpha(\omega) = -\frac{e}{E_o}\int Z\delta\rho(\mathbf{r},\omega)d\mathbf{r} \quad (12)$$

Note that $\alpha(\omega)$ like $\delta\rho(\mathbf{r},\omega)$ is complex. The induced density deviation (and also the corresponding induced potential) can have a phase difference with respect to that of the applied external field. Once $\alpha(\omega)$ is determined, the photoabsorption cross-section $\sigma(\omega)$ of the atom is obtained from

$$\sigma(\omega) = \frac{4\pi\omega}{c} Im\alpha(\omega) \quad (13)$$

2. Partial Cross-Sections

In order to see the connection with the IPA-model, consider the partial cross-section due to photoionization from a specific bound state $\psi_i(\mathbf{r})$ to a final continuum state $\psi_f(\mathbf{r})$. The initial atomic state is represented as

$$\psi_i(\mathbf{r}) = \frac{U_{nl}(r)}{r} Y_L(\hat{r}) \quad (14)$$

and the final continuum state with wavevector $\mathbf{K}$ and energy ϵ as

$$\psi_f(\mathbf{r}) = 4\pi \sum_{L'} A_{L'} i^{l'} \frac{P_{\epsilon l'}(r)}{r} Y^*_{L'}(\hat{K}) Y_{L'}(\hat{r}) \tag{15}$$

The complex coefficients $A'_l s$ are found by requiring $\psi_f(r)$ to behave asymptotically as an incident plane wave plus a spherical wave. Then the partial cross-section σ_{nl} is shown to be

$$\sigma_{nl}(\omega) = 2(2l+1)\alpha\hbar\omega\sqrt{\epsilon}a_B^2 \times \sum_{L'} |A^2_l| < l100|l'0 >|^2 \int P_{\epsilon l'}(r) V^{SCF}(r,\omega) U_{nl}(r) dr|^2 \tag{16}$$

where $< l100|l'0 >$ is a Clebsch-Gordon coefficient.

In Equation (16), $V^{SCF}(r,\omega)$ is a frequency dependent complex self-consistent potential. Note that if $V^{SCF}(r,\omega)$ is replaced by the usual dipole moment operator, one obtains the conventional or independent particle approximation (IPA) result. In actual calculations, both bound and continuum wave functions are generated numerically using the Numerov method for integrating the Dirac equation. Let us also note that the real and imaginary parts of the self-consistent field contribute to the partial cross-section without interference. Computations were performed for both the conventional independent particle model and the time-dependent linear response to density functional method for comparison purposes.

B. RESULTS

To see the usefulness of the linear response approximation within the density functional method, we first discuss the results for a few neutral atoms. The computed photoionization cross-section for neutral xenon as a function of photon energy near the 4d-threshold is shown in Figure 1. The results of the present method (Curve A) are compared with conventional IPA-model results (Curve B). It is seen that the IPA-model does not reproduce the experimental data[6] at all whereas the present model agrees very well with the experimental data over this range of photon energy, including the peak at about 7 Ryd. In that range, the IPA cross-section shows a rapid decrease which is in contrast to experimental data.

The reason for this difference in the two models arise from the polarization effect of the atom subject to the incident radiation. This collective effect is missing in the IPA calculation. A large number of electrons forming the atom participate in the polarization process. The external field is *screened* in the energy range 5 - 6 Ryd (and again in the range 8.5 - 9.5 Ryd), and is *antiscreened* in the intermediate 6 - 8 Ryd range. The antiscreening effect produces a stronger effective field for the 4d-electron to photoionize, thereby enhancing the cross-section in the intermediate range as seen in Figure 1.

The 3s-partial cross-section for argon is shown in Figure 2. The experimental data[7] in the range 30 - 65 eV are depicted by circles with error bars. The conventional IPA-model (Curve A) does not show the experimentally seen variation at all. The present response function method reproduces the observed variation including the Cooper minimum at about 43 eV. The occurrence of the Cooper minimum is known to be due to the vanishing of the matrix element between bound and continuum states at that photon energy. In the present model, the observed minimum in cross-section occurs because the induced potential almost exactly cancels out the external field, reducing the effective field to zero.

The *total* cross-section for an argon atom computed according to the present model also shows better agreement with experimental data[9] than the IPA, Hartree-Fock length and velocity results of Kennedy and Manson[8]. This is shown in Figure 3. The HF-velocity

approximation gives, for example, a cross-section twice as large at 40 eV whereas the HF-length result is six times larger than the experimental data at the same photon energy.

The results of our calculation for aluminum are given in Table II. Aluminum is of interest in many experimental studies and the data have to be provided by theoretical calculations. Substantial difference can be seen betwen calculated cross-sections generated by our present model and those from the IPA-model (Table II). The variation of the contribution of each electronic state to the total cross-section is also seen from Table II.

The results for neutral sodium are given in Table I. Both the present model and the IPA calculations show similar features; the cross-section drops in the photon energy range 5 - 7 eV, goes through the minimum and then rises gradually in the 8 - 11 eV range. This feature is seen experimentally and the data generated from our present model are in reasonable agreement with experimental observation.

Ions of specific configurations such as neon-like argon or lithium-like carbon are of interest for x-ray laser systems. No experimental data is available for these ions and thus the data have to be generated by theoretical calculations. The computed results for these ions are given in Tables III and IV. For neon-like argon, the collective polarization process discussed earlier is somewhat more effective than in lithium-like carbon because of the larger number of bound electrons in a neon-like ion. This contributes to the difference of the results from present model with the IPA calculations (Table III).

The results presented above are for single atoms or ions without the effect of the plasma environment. Such a description is appropriate for low density plasmas. For high density plasmas, however, a number of additional effects such as screening shifts of energy levels, modification of wave functions of bound and continuum wave functions as well as potentials of the multielectron ion embedded in the plasma have to be considered.

For proper treatment of these effects, the self-consistent two-component density functional method at finite temperatures[10] should be used. The important issue is to study the modifications of photoabsorption and other atomic cross-sections with variations of plasma density and temperature. Computations were performed for several hydrogenic

and lithium-like ions immersed in plasmas of densities and temperatures of interest to x-ray laser plasmas. The results of these calculations and their importance in overall modeling of x-ray lasers will be discussed in a seperate report.

C. LASER-ATOM INTERACTION

The linear response approximation within the density functional method is adequate for most experimental studies of photoabsorption processes of atoms or ions due to interaction with an applied radiation (such as lasers or synchrotron sources). In some experimental situations, however, the applied radiation can be very strong and can have electric field strengths comparable to atomic field strengths. Some of the recent experimental studies with high power, short pulsed lasers[12] have raised the possibility of development of x-ray lasers utilizing x-ray emission from excited, multiply-charged ions produced by multiphoton ionization processes, for example. A host of atomic physics issues arises in this context: for development of realistic theoretical models to interpret experimental observations, to investigate physical mechanisms for generating atomic core vacancies and associated x-ray fluorescence, coupling of collective modes to the radiation field and atomic cores etc. This is a new and complex field of research that requires several years of intensive effort to understand and correlate the effects involved.

To generalize beyond the linear response method, one approach is to utilize the Vashista-Singwi[11] scheme to calculate a new time-dependent (or frequency dependent) response function $\bar{\chi}(\omega)$ that includes higher order effects. It can be shown that this new generalized $\bar{\chi}(\omega)$ is related to the linear response function $\chi(\omega)$ of Equation (10) used previously by

$$\bar{\chi}(\omega) = \frac{\chi(\omega)}{1 - G(\omega)\chi(\omega)}. \tag{17}$$

The correction factor $G(\omega)$ that modifies the response function is determined by the appropriate structure factors. Calculations using this method has been performed for electron systems and are known to give improved results.

The other approach to treat non-linear effects in laser-atom interaction is via the full time-dependent Schröinger equation,

$$i\hbar \frac{\partial \psi(\mathbf{r},t)}{\partial t} = (H_{atom} + H_{int})\psi(\mathbf{r},t) \tag{18}$$

where $H_{int} = -e\mathbf{r}\cdot\mathbf{E}(t)$. Unlike linear response approximation, the interaction needs to be treated in a non perturbative fashion. The full numerical solution for the time-dependent wave function should be carried out, and the transition amplitudes for atomic processes can then be calculated. Some work in this direction has been done[13] and application has been made to atomic xenon. The probability of excitation of inner shell electrons by assuming coherently driven nonlinear motion of outer electronic shell (produced by the external laser radiation) was calculated with some simplifying assumption. An alternative approach to treat strong electric field problems is the functional integral method. This method is particularly suitable to calculate transition amplitudes when contributions of many excited atomic states are important as is the case for strong laser-atom processes. More work needs to be done in properly developing these techniques and in applying these to investigate the various physical processes mentioned earlier and to correlate with experimental observations.

III. CONCLUSIONS

It is demonstrated that the linear response scheme within the framework of density functional method can provide reliable atomic data for various atoms and ions of experimental interest. This model is particularly useful in those situations where conventional independent particle models fail to generate accurate data. The atomic stucture code for multielectron ions of arbitrary Z is of central importance in these calculations. Proper relativistic treatment is included in our work for high Z ions. The mechanism of time-dependent polarization of the atom is seen to be important in describing the experimental observations.

For most experimental situations, the present method is adequate and very useful. If the applied radiation field strength is very high, suitable generalization of the present model or developement of new techniques are necessary to treat those conditions. We have pointed out some of the approaches that are useful in this context.

REFERENCES

1 See, for example, U. Fano and J. W. Cooper, *Rev. Mod. Phys.* **40**, 441 (1956).

2 M. J. Stott and E. Zaremba, *Phys. Rev. A* **21**, 12 (1980).

3 A. Zangwill and P. Soven, *Phys. Rev. A* **21**, 1561 (1980).

4 D. Liberman and A. Zangwill, *Comput. Phys. Commun.* **32**, 75 (1984).

5 U. Gupta and A. K. Rajagopal, Review Article in *Phys. Reports* **82**, No. 6 (North Holland Publishing Co.) (1982).

6 R. Hansel, G. Keitel, P. Schriever and C. Kunz, *Phys. Rev.* **188**, 1375 (1969).

7 K. H. Tan and C. E. Brion, *J. Electron Spectros.* **13**, 77 (1978).

8 D. J. Kennedy and S. T. Manson, *Phys. Rev. A* **5**, 227 (1971).

9 J. A. R. Samson, *Advan. Atom. Mol. Phys.* **2**, 178 (1966).

10 U. Gupta, M. Blaha and J. Davis, *J. Phys. B* **17**, 3617 (1984).

11 P. Vashista and K. Singwi, *Phys. Rev. B* **6**, 875 (1972).

12 T. S. Luk, U. Johann, H. Egger, H. Pummer and C. K. Rhodes, *Phys. Rev. A* **32**, 214 (1985).

13 A. Szoke and C. K. Rhodes, *Phys. Rev. Lett.* **56**, No. 7, 720 (1986).

IV. TABLES

TABLE I

Neutral Sodium

Photon Energy(eV)	Electronic State	Photoionization Cross-Section (Megabarn)	
		IPA	Present Model
5.0	$3s_{1/2}$	0.2251	0.5641
5.5	"	0.0734	0.2222
6.0	"	0.0149	0.0719
7.0	"	0.0052	0.0000
8.0	"	0.0342	0.0220
9.0	"	0.0636	0.0576
10.0	"	0.0853	0.0873
10.2	"	0.0887	0.0922
10.5	"	0.0932	0.0989

TABLE II

Neutral Aluminum

Photon Energy(eV)	Electronic State	Photoionization Cross-Section (Megabarn)	
		IPA	Present Model
460	$2s_{1/2}$	0.1069	0.1191
	$2p_{1/2}$	0.0806	0.0977
	$2p_{3/2}$	0.1594	0.1933
	$3s_{1/2}$	0.0081	0.0089
	$3p_{1/2}$	0.0041	0.0046
	Total	0.3592	0.4236
510	2s1/2	0.0890	0.0986
	$2p_{1/2}$	0.0604	0.0724
	$2p_{3/2}$	0.1193	0.1431
	$3s_{1/2}$	0.0063	0.0070
	$3p_{1/2}$	0.0012	0.0014
	Total	0.2761	0.3225
580	$2s_{1/2}$	0.0702	0.0772
	$2p_{1/2}$	0.0418	0.0493
	$2p_{3/2}$	0.0825	0.0974
	$3s_{1/2}$	0.0049	0.0054
	$3p_{1/2}$	0.0004	0.0006
	Total	0.1998	0.2298
600	$2s_{1/2}$	0.0658	0.0723
	$2p_{1/2}$	0.0379	0.0445
	$2p_{3/2}$	0.0748	0.0878
	$3s_{1/2}$	0.0047	0.0052
	$3p_{1/2}$	0.0023	0.0025
	Total	0.1854	0.2123

TABLE II CONTINUED

	$2s_{1/2}$	0.0489	0.0530
	$2p_{1/2}$	0.0240	0.0276
700	$2p_{3/2}$	0.0474	0.0544
	$3s_{1/2}$	0.0036	0.0039
	$3p_{1/2}$	0.0014	0.0015
	Total	0.1253	0.1404

TABLE III

Neon - like Argon

Photon Energy(eV)	Electronic State	Photoionization Cross-Section (Megabarn)	
		IPA	Present Model
395	$2p_{3/2}$	1.0061	0.9481
	$2p_{1/2}$	0.4984	0.5060
400	$2p_{3/2}$	0.9905	1.0065
	Total	1.4889	1.5125
	$2p_{1/2}$	0.3952	0.4183
440	$2p_{3/2}$	0.7807	0.8273
	Total	1.1759	1.2457
	$2s_{1/2}$	0.1981	0.2073
480	$2p_{1/2}$	0.3188	0.3471
	$2p_{3/2}$	0.6297	0.6863
	Total	1.1466	1.2407
	$2s_{1/2}$	0.1901	0.1995
500	$2p_{1/2}$	0.2867	0.3159
	$2p_{3/2}$	0.5656	0.6239
	Total	1.0424	1.1393
	$2s_{1/2}$	0.1682	0.1776
540	$2p_{1/2}$	0.2368	0.2657
	$2p_{3/2}$	0.4668	0.5243
	Total	0.8719	0.9676

TABLE III CONTINUED

560	$2s_{1/2}$	0.1497	0.1589
	$2p_{1/2}$	0.1971	0.2240
	$2p_{3/2}$	0.3884	0.4419
	Total	0.7351	0.8247
600	$2s_{1/2}$	0.1422	0.1513
	$2p_{1/2}$	0.1804	0.2063
	$2p_{3/2}$	0.3553	0.4068
	Total	0.6779	0.7643

TABLE IV

Lithium - like Carbon

Photon Energy(eV)	Electronic State	Photoionization Cross-Section (Megabarn)	
		IPA	Present Model
250	$2s_{1/2}$	0.0424	0.0370
300	$2s_{1/2}$	0.0280	0.0275
	$1s_{1/2}$	0.5968	0.5969
350	$2s_{1/2}$	0.0193	0.0190
	Total	0.6161	0.6159
	$1s_{1/2}$	0.4354	0.4444
400	$2s_{1/2}$	0.0141	0.0141
	Total	0.4495	0.4585
	$1s_{1/2}$	0.3088	0.3203
460	$2s_{1/2}$	0.0100	0.0101
	Total	0.3188	0.3304
	$1s_{1/2}$	0.2499	0.2613
500	$2s_{1/2}$	0.0081	0.0083
	Total	0.2580	0.2695
	$1s_{1/2}$	0.1954	0.2059
550	$2s_{1/2}$	0.0065	0.0066
	Total	0.2019	0.2125
	$1s_{1/2}$	0.1556	0.1650
600	$2s_{1/2}$	0.0051	0.0053
	Total	0.1608	0.1703

V. FIGURES

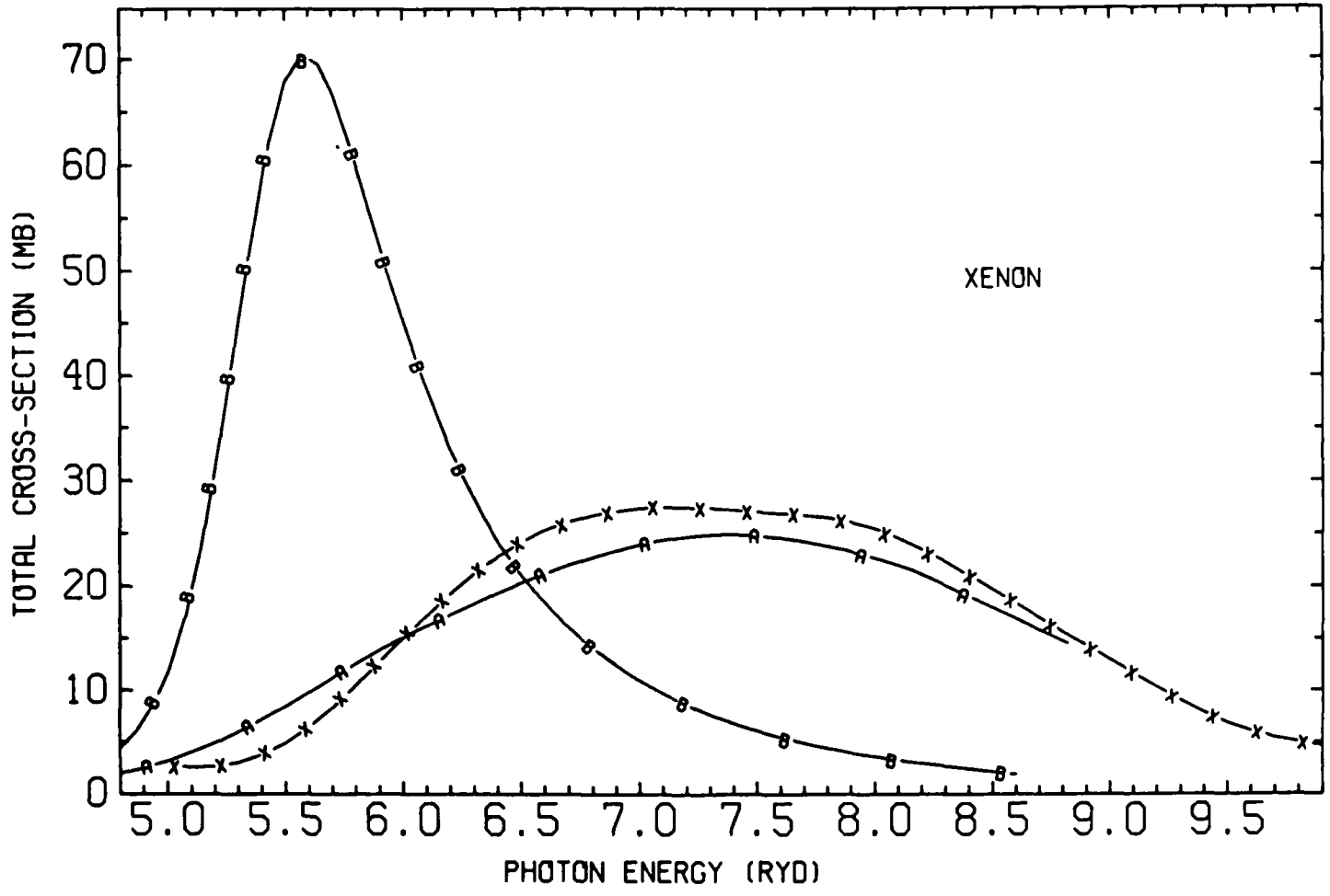

TOTAL PHOTOIONIZATION CROSS-SECTION OF NEUTRAL XENON NEAR 4D THRESHOLD. CURVE A: TIME DEPENDENT DENSITY FUNCTIONAL CALCULATION. CURVE B: INDEPENDENT PARTICLE MODEL. EXPERIMENTAL DATA FROM R. HANSEL ET. AL., PHYS. REV. 188, 1375 (1969)

Figure 1

FIG. 1

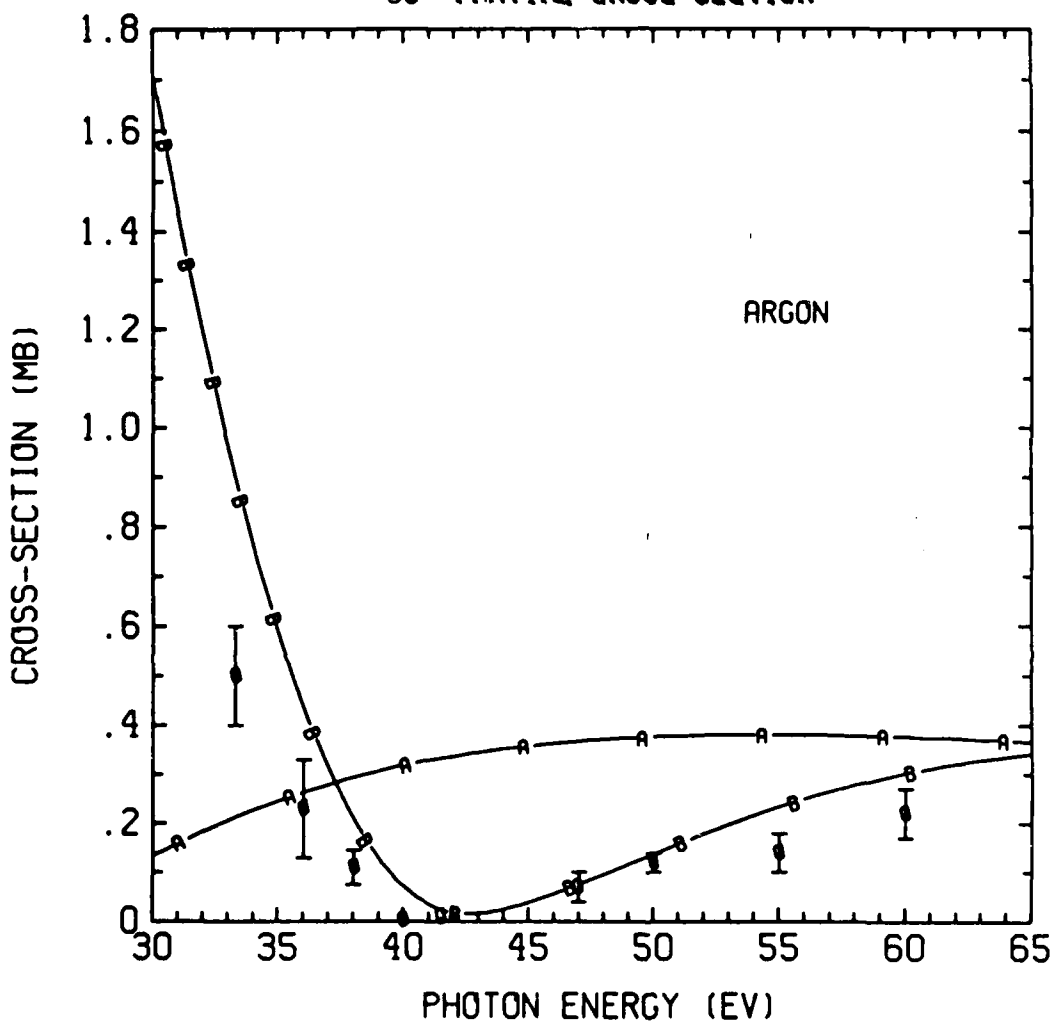

CURVE A: INDEPENDENT PARTICLE MODEL.

CURVE B: TIME-DEPENDENT DENSITY FUNCTIONAL CALCULATION.

DATA FROM K. TAN & C. BRION, J. ELECTRON SPECTROS. 13, 77(1978).

Fig. 2

Figure 2

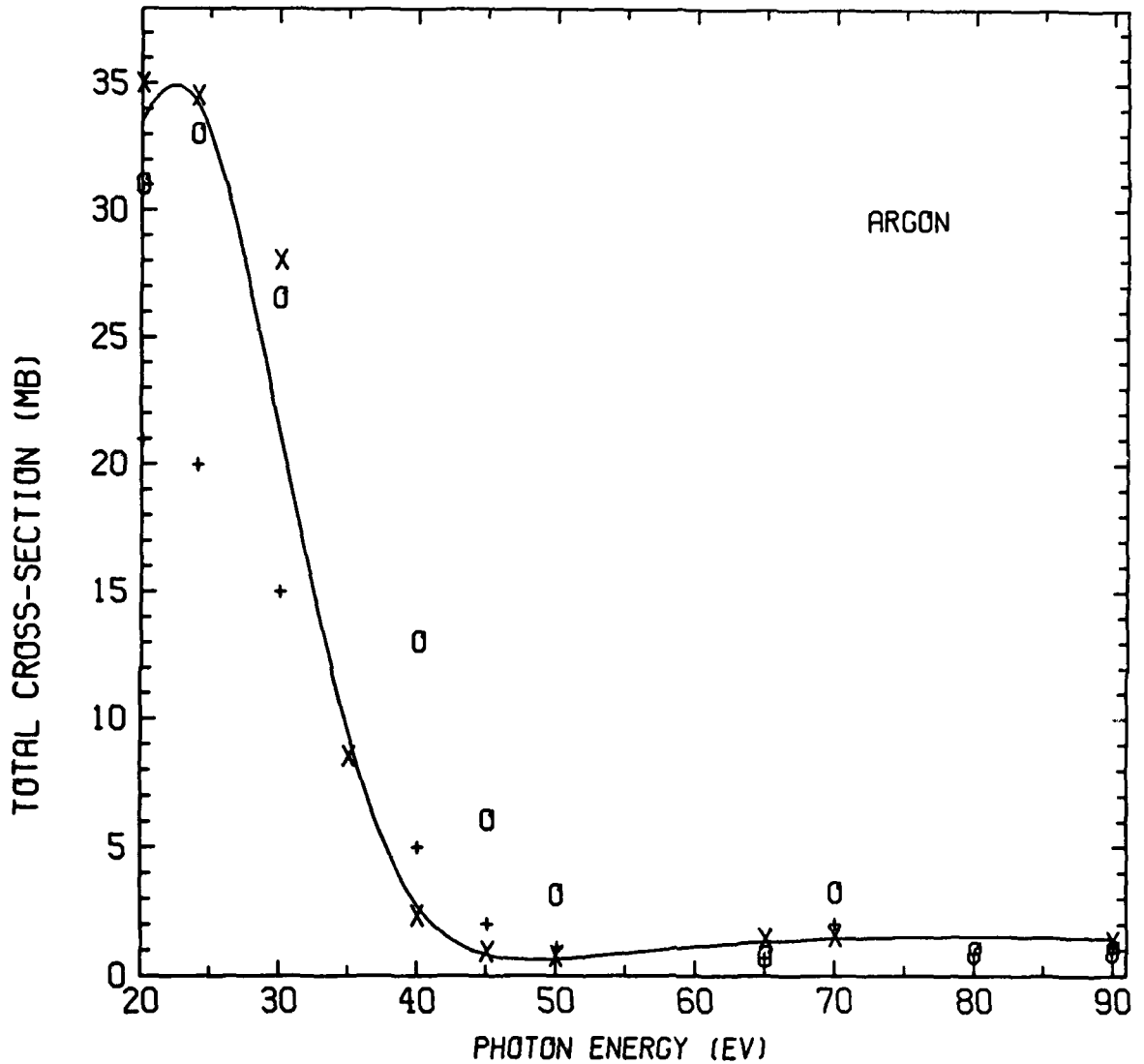

SOLID CURVE: TIME-DEPENDENT DENSITY FUNCTIONAL CALCULATION.
X: EXPERIMANTAL DATA FROM J.A.R.SAMSON, ADVAN. ATOM. MOL. PHYS. 2, 178(1966). +: HARTREE-FOCK (VELOCITY APPROX.) AND
O: HARTREE-FOCK (LENGTH APPROX.) BY KENNEDY & MANSON, PHYS. REV. A 5, 227(1972).

FIG.3

Figure 3

END

DATE

FILMED

8-88

DTIC